

532.542

Paper No. 157-13

## Asymmetric Swirling Flows in Composite Pipe Bends \*

By Mitsukiyo MURAKAMI\*\* and Yukimaru SHIMIZU\*\*\*

When a non-uniform flow accompanied with a secondary circulation enters a bend, there develops an oscillatory or spiral type of secondary flow. In this paper, this type of flow is studied theoretically and the results are compared with the experiments.

## 1. Introduction

If a fluid with a non-uniform velocity distribution resulting from a curved motion in a bend is introduced into another bend located in a twisted S form to the first bend, an oscillatory type of secondary flow may appear in the second bend. This secondary flow is attributed to the effects of the unbalanced centrifugal force due to the non-uniform distribution of main flow velocities. This flow has been studied by several investigators. Squire and Winter<sup>(1)</sup> showed theoretically that a transverse secondary circulation was caused in a bend when a non-uniform flow was introduced into the bend. Considering a shear flow type of non-uniform velocity distribution at the bend inlet, Hawthorne<sup>(2)</sup> solved an oscillatory spiral motion of fluid flow appearing in a large bend of constant radius. Assuming that the flow is inviscid and incompressible, Horlock<sup>(3)</sup> analyzed the general behaviour of the secondary flow in a bend in which the radius of curvature is repeatedly reversed.

When two bends are combined in a twisted S form, the outlet velocity has a non-uniform profile due to a secondary circulation. If this deformed flow is introduced into the next bend located downstream, an oscillatory or spiral type of secondary flow will occur in the downstream bend.

In this paper this type of flow is analyzed theoretically and experimentally.

## 2. Nomenclature

$d$  : diameter of pipe  
 $L_{m1}$  : length of the spacer between the first and second bends (Fig.2)  
 $L_{m2}$  : length of the spacer between the second and third bends (Fig.2)  
 $M'$  : dimensionless angular momentum flux, Eq. (39)  
 $p$  : static pressure  
 $r_0$  : pipe radius,  $= d/2$   
 $r$  : radial distance,  $r' = r/r_0$   
 $R$  : radius of curvature (Fig.1)  
 $r_c$  : radial distance to the eccentric centre (Fig.2(b), Eq. (36))  
 $s$  : distance along a bend axis from the inlet,  $s' = s/d$

$U$  : mean axial velocity  
 $U_z$  : axial velocity  
 $\bar{U}$  : maximum axial velocity  
 $u$  : axial component of perturbation velocity  
 $V$  : peripheral velocity  
 $v$  : peripheral component of perturbation velocity  
 $W$  : radial velocity  
 $w$  : radial component of perturbation velocity  
 $U_z'$  : dimensionless axial velocity,  $= U_z/U$   
 $v'$  : dimensionless peripheral velocity,  $= v/U$   
 $\alpha$  : angular position of maximum axial velocity gradient measured from the bend plane in clockwise direction (P axis(+), Fig.1)  
 $\alpha_0$  : value of  $\alpha$  at the bend inlet, Fig.1  
 $\gamma$  : angular position in a bend section measured from the bend plane in clockwise direction, Fig.1  
 $\theta$  : angle between a bend section and the bend inlet, Fig.1  
 $\theta_0$  : total deflection angle of a bend, Fig.1  
 $\psi$  : angle of pipe line bent by the first and the second bends, Fig.2(a)  
 $\phi$  : angle of pipe line bent by the second and the third bends, Fig.2(a)  
 $\epsilon$  : absolute roughness of bend wall  
 $\xi$  : axial component of perturbation vorticity  
 $\eta$  : peripheral component of perturbation vorticity  
 $\zeta$  : radial component of perturbation vorticity  
 $\Omega_0$  : inlet vorticity at  $\theta=0^\circ$  section  
 $\Omega_0'$  : dimensionless value of  $\Omega_0$ ,  $= \Omega_0 r_0 / U$   
 $\rho$  : density of fluid  
 $\nu$  : kinematic viscosity

## 3. Theory

The theory will be presented for a steady, inviscid and incompressible flow without body forces. With the co-ordinate system shown in Fig.1, the Euler equations of motion for the flow in a curved duct may be written as

$$-\frac{1}{\rho R} \frac{\partial p}{\partial \theta} = w \frac{\partial(U+u)}{\partial r} + \frac{v^*}{r} \frac{\partial(U+u)}{\partial \gamma} + \frac{U+u}{R} \frac{\partial(U+u)}{\partial \theta} + \frac{(U+u)}{R} \times \{w \sin \gamma + v^* \cos \gamma\} \quad (1)$$

$$-\frac{1}{\rho r} \frac{\partial p}{\partial \gamma} = w \frac{\partial v^*}{\partial r} + \frac{v^*}{r} \frac{\partial v^*}{\partial \gamma} + \frac{U+u}{R} \frac{\partial v^*}{\partial \theta} + \frac{w v^*}{r} - \frac{(U+u)^2 \cos \gamma}{R} \quad (2)$$

$$-\frac{1}{\rho} \frac{\partial p}{\partial r} = w \frac{\partial w}{\partial r} + \frac{v^*}{r} \frac{\partial w}{\partial \gamma} + \frac{U+u}{R} \frac{\partial w}{\partial \theta} - \frac{v^{*2}}{r} - \frac{(U+u)^2 \sin \gamma}{R} \quad (3)$$

\* Received 4th November, 1975.

\*\* Professor, Faculty of Engineering, Nagoya University.

\*\*\* Associate Professor, Faculty of Engineering, Mie University, Kamihamacho, Tsu, Mie, Japan.

and the continuity equation is

$$\frac{1}{R} \frac{\partial u}{\partial \theta} + \frac{1}{r} \frac{\partial v^*}{\partial \gamma} + \frac{1}{r} \frac{\partial (rw)}{\partial r} = 0 \quad (4)$$

in which it is assumed that (1):  $r/R$  is so small that  $(r/R)^2$  may be neglected, (2): there are a non-uniform distribution of axial velocities and a weak swirling velocities at the bend inlet, (3): the perturbation velocity components  $u$  and  $v$  are small compared with the mean axial velocity  $U$ .

Vorticity components due to the perturbation velocities,  $\xi$ ,  $\eta$  and  $\zeta$  in  $X$ ,  $Y$  and  $Z$  directions, respectively, can be written as

$$\xi = -\frac{1}{r} \left[ \frac{\partial (v^* r)}{\partial r} - \frac{\partial w}{\partial \gamma} \right] \quad (5a)$$

$$\eta = -\frac{1}{R} \frac{\partial w}{\partial \theta} + \frac{(U+u) \sin \gamma}{R} + \frac{\partial (U+u)}{\partial r} \quad (5b)$$

$$\zeta = -\frac{1}{r} \frac{\partial (U+u)}{\partial \gamma} - \frac{(U+u) \cos \gamma}{R} + \frac{1}{R} \frac{\partial v^*}{\partial \theta} \quad (5c)$$

The stagnation pressure in a bend section is

$$p_0 = p + \frac{1}{2} \rho [(U+u)^2 + v^{*2} + w^2] \quad (6)$$

Using  $\partial p_0 / \partial \theta$ , which is derived from Eq. (6), together with Eqs. (5b) and (5c), Equation (1) may be expressed as follows:

$$\frac{1}{\rho R} \frac{\partial p_0}{\partial \theta} = \frac{1}{R} \frac{\partial}{\partial \theta} \left( \frac{p}{\rho} \right) + (U+u) \frac{\partial u}{\partial \theta} = v^* \zeta - w \eta \quad (7)$$

The right-hand side of Eq. (7) involves the products of perturbation terms only, hence, the following is obtained as the first order approximation

$$\frac{\partial p_0}{\partial \theta} = 0 \quad (8)$$

If the fluid viscosity is neglected, the distribution of axial velocities remains unaltered in  $\theta$ -direction, hence,

$$\frac{\partial p}{\partial \theta} = 0 \quad (9)$$

In this analysis assuming that the perturbation velocity  $u$  changes linearly in the downward direction as shown in Fig. 1, the profile at any section downstream may be expressed as

$$u = \Omega_0 r \cos (\gamma - \alpha) \quad (10)$$

where  $\Omega_0$  is the inlet vorticity at  $\theta = 0^\circ$  section. Eliminating  $p$  from Eqs. (2) and (3) and using Eq. (5),

$$\begin{aligned} -\frac{\partial \xi}{\partial \theta} &= \frac{\partial}{\partial \theta} \left( \frac{1}{r} \frac{\partial}{\partial r} (r v^*) - \frac{1}{r} \frac{\partial w}{\partial \gamma} \right) \\ &= 2 \left( \cos \gamma \frac{\partial u}{\partial r} - \frac{\sin \gamma}{r} \frac{\partial u}{\partial \gamma} \right) \end{aligned} \quad (11)$$

Substituting Eq. (10) into Eq. (11)

$$\frac{d\xi}{d\theta} = -2\Omega_0 \cos \alpha \quad (12)$$

As  $\alpha$  changes in  $\theta$ -direction only,  $\xi$  may be expressed as a function of  $\theta$ . With this fact in mind and using the condition of  $\partial u / \partial \theta = 0$ , Eqs. (4) and (5a) can be solved to give

$$v^* = -\frac{1}{2} r \xi, \quad w = 0 \quad (13)$$

The differential equation of a streamline is given by

$$\frac{dr}{w} = \frac{r d\alpha}{v^*} = \frac{R d\theta}{U+u} \quad (14)$$

Substituting Eq. (14) into Eq. (13) gives

$$\frac{d\alpha}{d\theta} = \frac{R}{r} \frac{v^*}{U+u} \quad (15)$$

$$\frac{d\alpha}{d\theta} = -\frac{R}{2} \frac{\xi}{U+u} \quad (16)$$

Differentiating both sides of Eq. (16) by  $\theta$  and employing the relationship of Eq. (12), the following expression is obtained

$$\frac{d^2 \alpha}{d\theta^2} = \frac{R \Omega_0}{U+u} \cos \alpha \quad (17)$$

If the maximum axial velocity at the position,  $\gamma = \alpha$  and  $r = d/2$ , is denoted by  $\bar{U}$ , the vorticity at the inlet section is given by

$$\Omega_0 = \frac{\bar{U} - U}{r_0} \quad (18)$$

Putting  $\Omega_0 r_0 / U = \Omega'_0$ , Eq. (18) gives

$$\bar{U} = (1 + \Omega'_0) U \quad (19)$$

Substituting the relationship of  $U + (u)_{r=d/2} = \bar{U}$  in Eq. (17) and using Eqs. (18) and (19), the equation governing the maximum axial velocity point can be derived as

$$\frac{d^2 \alpha}{d\theta^2} = \frac{R}{d} \frac{2\Omega'_0}{1 + \Omega'_0} \cos \alpha \quad (20)$$

Putting  $\alpha' = \alpha - \pi/2$  and

$$k = \frac{R}{d} \frac{2\Omega'_0}{1 + \Omega'_0} \quad (21)$$

the above equation (20) becomes

$$\frac{d^2 \alpha'}{d\theta^2} = -k \sin \alpha' \quad (22)$$

With use of the centre line length of the bend expressed by

$$s = \theta R = s' d \quad (23)$$

the differential equation (22) may be rearranged as

$$\left( \frac{R}{d} \right)^2 \frac{d^2 \alpha'}{ds'^2} = -k \sin \alpha' \quad (24)$$

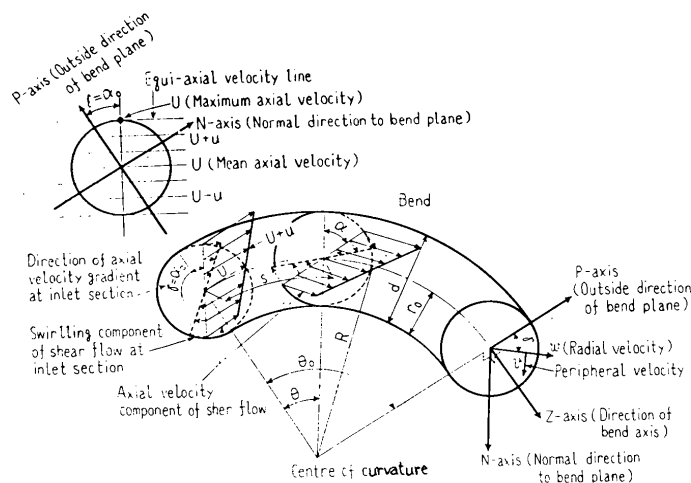


Fig. 1 Co-ordinates for bend duct and velocity distribution at bend inlet

Integration of this equation gives

$$\frac{d\alpha'}{ds'} = \sqrt{\left(\frac{d\alpha'}{ds'}\right)^2_{s'=0} + \frac{4}{k} \left(\frac{2Q_0'}{1+Q_0'}\right)^2 \left\{ \sin^2\left(\frac{\alpha'}{2}\right)_{s'=0} - \sin^2\frac{\alpha'}{2} \right\}} \quad (25)$$

With the initial conditions that  $d\alpha'/ds' = \xi_0$  and  $\alpha = \alpha_0 (= \alpha_0'_{s'=0})$  at  $s=0$ ,  $\xi_0$  is the vorticity component assumed to be disturbed uniformly over the inlet section, and  $v_0 = (1/2)r\xi_0$ , Eq. (25) can be integrated again to give

$$s' = \int_{\alpha_0'}^{\alpha'} \frac{d\alpha'}{\sqrt{\xi_0^2 + \frac{4}{k} \left(\frac{2Q_0'}{1+Q_0'}\right)^2 \sin^2\frac{\alpha_0'}{2} \left\{ 1 - \frac{(4/k) \cdot 2Q_0'/(1+Q_0')^2}{\xi_0^2 + (4/k) \cdot 2Q_0'/(1+Q_0')^2 \sin^2(\alpha_0'/2)} \sin^2\frac{\alpha'}{2} \right\}}} } \quad (26)$$

or

$$s' = \frac{1}{\sqrt{B}} \int_{\alpha_0'}^{\alpha'} \left( \frac{d\alpha'}{\sqrt{1 - \frac{4}{KB} \sin^2\frac{\alpha'}{2}}} \right) \quad (27)$$

where

$$K = \frac{R}{d} \frac{1+Q_0'}{2Q_0'} = \frac{1}{2} \left( \frac{1+Q_0'}{2Q_0'} \right)^2, \quad B = \xi_0^2 + (4/K) \sin^2\frac{\alpha_0'}{2} \quad (28)$$

Equation (27) has the following three solutions:

(a) When  $4/KB > 1$ :

The equation is an elliptic integral of the first kind and is expressed as

$$s' = \sqrt{K} \int_{\alpha_0'}^{\alpha'} \left( \frac{d\alpha'}{\sqrt{1 - \sin^2\frac{\alpha'}{2} \sin^2\tau}} \right) \quad (29)$$

where

$$\sin^2\frac{\alpha'}{2} = KB \sin^2\tau, \quad \sin\frac{\alpha_0'}{2} / \sin\frac{\alpha'}{2} = \sin\tau$$

Equation (29) can be solved for  $\alpha'$  to give

$$\alpha' = 2 \sin^{-1} \left[ \sin\frac{\alpha_0'}{2} \sin(s'/\sqrt{K}) \right] = 2 \sin^{-1} \left[ \sin\frac{\alpha_0'}{2} \sin \left\{ \theta \times (R/d) / \sqrt{K} \right\} \right] \quad (30)$$

from which it is seen that  $\alpha'$  is a periodic function of  $s'$ . Thus, in the bend, the secondary flow is not spiral but oscillatory, and the direction of the circulation varies periodically towards the downstream; in other words, the flow is called an oscillatory swirling flow.

(b) When  $4/KB < 1$ :

The right-hand side of Eq. (27) is written as

$$F(\alpha') = \int_{\alpha_0'}^{\alpha'} \left( \frac{d\alpha'}{\sqrt{1 - (4/KB) \sin^2\frac{\alpha'}{2}}} \right)$$

This may be expanded in a series in terms of  $(4/KB) \sin^2(\alpha'/2)$  to give

$$F(\alpha') = \left[ \left( 1 + \frac{a_1}{2} + \frac{3}{8} a_2 + \frac{5}{16} a_3 \right) \frac{\alpha'}{2} - \left( \frac{a_1}{4} + \frac{a_2}{4} + \frac{15}{64} a_3 \right) \sin \alpha' + \left( \frac{a_2}{32} + \frac{3}{64} a_3 \right) \sin 2\alpha' - \frac{a_3}{192} \sin 3\alpha' \right]_{\alpha_0'}^{\alpha'} \quad (31)$$

where

$$a_1 = \frac{1}{2} \frac{4}{KB}, \quad a_2 = \frac{1 \cdot 3}{2 \cdot 4} \left( \frac{4}{KB} \right)^2, \quad a_3 = \frac{1 \cdot 3 \cdot 5}{2 \cdot 4 \cdot 6} \left( \frac{4}{KB} \right)^3$$

With these results, Eq. (27) yields the following expression

$$s' = \frac{1}{\sqrt{B}} F(\alpha') \quad (32)$$

$$\text{or} \quad \theta = \frac{1}{\sqrt{B}} \left( \frac{d}{R} \right) F(\alpha') \quad (33)$$

From these relations it is seen that  $\alpha'$  increases with an increase of  $s'$  or the distance along the bend axis from the bend inlet. Consequently, the direction of the circulation remains unaltered and a spiral type of secondary flow or spiral swirling flow is obtained in the bend.

(c) When  $4/KB = 1$ :

In this case, the integration of Eq. (27) gives

$$s' = -\frac{2}{\sqrt{B}} \ln \left| \frac{\tan\left(\frac{\alpha'}{4} + \frac{\pi}{4}\right)}{\tan\left(\frac{\alpha_0'}{4} + \frac{\pi}{4}\right)} \right| \quad (34)$$

$$\text{or} \quad \theta = -\frac{2}{\sqrt{B}} \left( \frac{d}{R} \right) \ln \left| \frac{\tan\left(\frac{\alpha'}{4} + \frac{\pi}{4}\right)}{\tan\left(\frac{\alpha_0'}{4} + \frac{\pi}{4}\right)} \right| \quad (35)$$

Thus, it follows that the angle  $\alpha'$  approaches asymptotically to  $180^\circ$  as  $s'$  increases. In this case the point of maximum axial velocity

moves asymptotically to the inside of bend section and the secondary rotation comes to stop in the bend.

#### 4. Experimental apparatus and procedure

The configuration of the pipe line employed in this experiment is shown in Fig. 2.

Three pipe bends are used, and each bend has a deflection angle  $\theta = 90^\circ$ . A fully developed velocity profile at the first

bend inlet is secured by taking the inlet tangent sufficiently long. This uniform flow will be disturbed in the bend, and at its outlet section the centre of flow velocities is shifted from the pipe axis towards the outside of the bend section. When this disturbed flow enters the second bend located close in a twisted S form, a centrifugal force acting on the flow in the second bend will cause a strong secondary circulation as well as non-uniform axial velocity distributions.

If the third bend is located in this non-uniform flow section, the inlet flow to the third bend will be a flow of non-uniform axial velocity distributions accompanied by a swirling component. The present analysis corresponds to this type of flow. To get a strong swirling flow, two upstream bends (the first and second bends) are located close to each other in a twisted S form, namely,  $\psi = 90^\circ$  and  $L_m = 0$ . The third bends are combined with the second in the state of  $L_m = 0$  and  $\phi = 0^\circ, 90^\circ$  and  $180^\circ$ , respectively. For these cases, at the inlet of the third bends, the angular and radial positions of axial velocity centre,  $\alpha_0$  and  $r/r_0$ , and the gradient of axial velocity distribution  $\Omega'_0$  are shown in Table 1, the results in which corresponding to those for bends of deflection angle of  $90^\circ$ .

To examine flow behaviour in a bend for the case when its inlet velocity has non-uniform axial profiles but no swirling components,

experiments were performed with pipe lines of bend angles of  $\psi = 45^\circ, 90^\circ$  and  $135^\circ$ , and spacer length of  $L_m = 0$ . Conditions of the inlet flow for the second bends,  $\xi'_0, \alpha_0, r/r_0$  and  $\Omega'_0$  in these cases are given in Table 2. Velocity distributions in the second bend, a deflection angle of which was  $180^\circ$ , were measured at sections of  $\theta = 0^\circ, 45^\circ, 90^\circ, 135^\circ$  and  $180^\circ$ , respectively.

To investigate the effects of bend curvature, three bends with  $R/d = 1.5, 2$  and  $3$  were employed in the experiments. The bends were of bronze casting and the relative roughness of the inside surface was  $\epsilon/d = 0.0035$  approximately.

#### 5. Definitions of flow centre and vorticity

##### 5.1 Flow centre

Non-uniformity of axial velocities in real flow does not change linearly as in a pure shearing flow, Fig. 1, and the angular

and radial positions of the eccentric centre of the non-uniform velocity distributions,  $\alpha$  and  $r_c$ , are defined by the following formulae

$$r_c = \sqrt{r_{xc}^2 + r_{yc}^2} \quad (36)$$

$$\text{and } \alpha = \tan^{-1}(r_{yc}/r_{xc}) \quad (37)$$

The values of  $r_{xc}$  and  $r_{yc}$  in the above equations correspond to the centre of momentum fluxes about the axes P-P and N-N as given by

$$\left. \begin{aligned} \frac{r_{xc}}{r_0} &= \frac{1}{\pi} \int_0^{2\pi} \int_0^1 U_z' r'^2 \sin \gamma d\gamma dr' \\ \frac{r_{yc}}{r_0} &= \frac{1}{\pi} \int_0^{2\pi} \int_0^1 U_z' r'^2 \cos \gamma d\gamma dr' \end{aligned} \right\} \quad (38)$$

where  $U_z'$  is a measured value of axial velocity component expressed dimensionlessly.

## 5.2 Vorticity and angular momentum flux

To find the value of vorticity  $\xi$  in a section, angular momentum of flow through a bend as defined by the following equation is considered

$$M' = \frac{2}{\pi} \int_0^{2\pi} \int_0^1 r'^2 U_z' V' dr' d\gamma \quad (39)$$

where  $V'$  is a dimensionless expression of the measured peripheral velocity. To represent the real axial velocity distribution, a linear relationship expressed by Eq. (10) is used as an approximation, and the following expressions are derived

$$\left. \begin{aligned} U_z' &= (U + u) : U = 1 + 2\alpha' r' \cos(\gamma - \alpha) \\ V' &= v' : U = \frac{1}{2} \xi' r' \end{aligned} \right\} \quad (40)$$

where

$$\xi' = \xi r_0 / U$$

With these relations, Eq. (39) yields

$$M' = \frac{2}{\pi} \int_0^{2\pi} \int_0^1 r'^2 [1 + 2\alpha' r' \cos(\gamma - \alpha)] \times \frac{1}{2} r' \xi' dr' d\gamma = \frac{1}{2} \xi' \quad (41)$$

At the inlet section of bends ( $\theta=0^\circ$ ),  $\alpha=\gamma$ , and

$$M_0' = \frac{1}{2} \xi_0' \quad (42)$$

Thus, the value of vorticity in a section can be obtained by use of angular momentum fluxes in Eqs. (41) and (42).

## 6. Comparison of theory and experiments

### 6.1 Entry of non-uniform axial flow with swirling velocity component

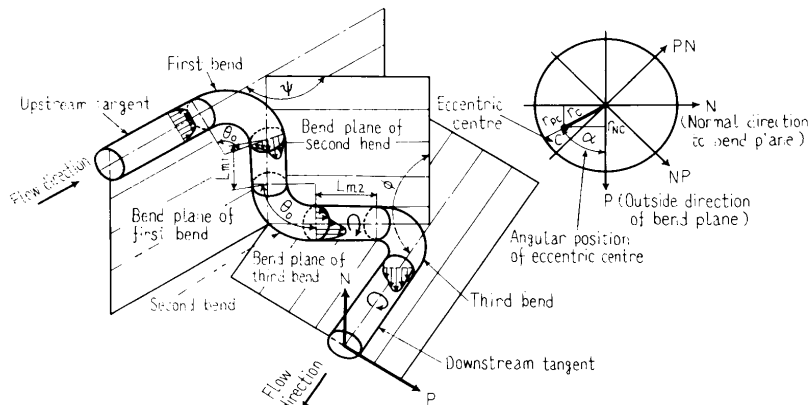


Fig.2 Notation of pipe bends

Axial velocity distributions in the second and third bends are shown in Fig.3, when two or three  $90^\circ$  bends are located close to each other in a twisted S form. The non-dimensional expressions of Eq. (10),  $u/U = (\Omega_0 r/U) \cos(\gamma - \alpha) = \Omega_0' \cos(\gamma - \alpha)$ , are also shown for  $\Omega_0' = 0.3, 0.6$  and  $1$ , respectively, in order to compare with the measured axial velocity distributions in Fig.3. With measured velocities, the values of  $K$  and  $B$  at the bend inlet can be calculated from Eqs. (37) and (42). The results are indicated in Fig.4, where the curves for  $4/KB=1$  ( $\Omega_0'=0.6$ ) corresponding to the case (c) discussed in section 3 are also shown. In this figure, symbol  $\bullet$  designates the experimental value at the second bend outlet when two bends were employed, and symbols  $\times, \circ, \Delta$  and  $\square$  the values at the third bend inlet when three bends were used (refer to Table 1). Each value  $\xi_0'$  of  $\bullet$  symbol corresponds to one when the swirling flow generated in the second bend becomes the strongest for each bend curvature ( $R/d$ ).

#### 6.1.1 Oscillatory swirling flow ( $4/KB > 1$ )

Velocity distributions in the third bend are shown in Fig.5, when three bends (each bend has a deflection angle of  $\theta_0=90^\circ$  and bend radius of  $R/d=2$ ) are combined in a state of  $\psi=90^\circ$  and  $\phi=0^\circ$  and  $L_{m1}=L_{m2}=0$ . The values of  $\alpha_0, \xi_0', R/d$  and  $\Omega_0' (=0.6)$  for this combination are given in Table 1, from which it is seen that  $4/KB=2.4$ . In this case the flow, which will be expected to occur by the present theory, must be an oscillatory swirling one. This was confirmed by experiments as shown in Fig.5, where the angular position of eccentric centre  $\alpha$  changes from  $27^\circ$  at the bend inlet  $\theta=0^\circ$  to  $68^\circ$  at  $\theta=45^\circ$  and to  $90^\circ$  at  $\theta=90^\circ$ , which shows an oscillatory spiral motion along the bend axis. With these values of  $R/d, \alpha_0, \xi_0'$  and  $\Omega_0'$  the relationship between  $\alpha$  and  $\theta$  can be obtained from Eq. (30) as shown in Fig.6, where the results are calculated with the same constants, but with different values of  $\Omega_0'$ . The experimental values expressed by a symbol  $\times$  show nearly the same tendency with the curve for  $\Omega_0'=0.8$ . The oscillatory nature of flow is also confirmed in Fig.5. A clockwise secondary circulation dominates at the bend inlet  $\theta=0^\circ$ , but it is weakened at the downstream section of  $\theta=45^\circ$  and at the section of  $\theta=90^\circ$  a counter-clockwise secondary circulation is developed.

#### 6.1.2 Spiral swirling flow ( $4/KB < 1$ )

Figure 7 shows the velocity distributions in the third bend, when three bends, dimensions of which are the same as in the above case, are combined in a state of  $\psi=90^\circ, \phi=180^\circ$ , and  $L_{m1}=L_{m2}=0$ . In this case, the value  $4/KB$  becomes  $0.7$  at the third bend inlet, when the values of  $\alpha_0, \xi_0', R/d$  and  $\Omega_0' (=0.6)$  are given in Table 1, and the condition for a spiral

swirling flow, namely  $4/KB < 1$ , is satisfied. Occurrence of this spiral flow is confirmed by examining the velocity distributions in Fig.7, where the angular position of velocity centre  $\alpha$  is seen to increase continuously along the bend axis, showing also one directional (clockwise) swirling secondary motion. With the values of  $\alpha_0$  and  $\xi'_0$  which can be found from the above results, Eq.(33) yields a relation between  $\alpha$  and  $\theta$  as shown in Fig.8, where the experimental values are also plotted. Agreement between the theory and experiments is qualitatively fair, and it becomes progressively poor as the flow approaches the outlet section. This discrepancy will be due to the pressure variation caused by centrifugal forces within a bend section, which is neglected in this theory for the sake of simplicity.

### 6.1.3 Suspended swirling flow ( $4/KB=1$ )

In a particular case, where three bends are suitably combined so as to satisfy the condition of  $4/KB=1$  at the third bend inlet; the swirling motion which would otherwise be observed at its inlet should cease in the third bend. This condition, however, could not be realized in the present experiment.

$\psi^\circ$	90		
$\phi^\circ$	0	90	180
$\alpha_0^\circ$	27	126	190 or -170
$\xi'_0$	0.74	0.74	0.74
$r_c/r_0$	0.043	0.034	0.054
$\Omega'_0$	0.3~0.6	0.3~0.6	0.3~0.6
R/d	2	2	2

Table 1 Direction of axial velocity gradient( $\alpha_0$ ), vorticity( $\xi'_0$ ), radial distance of eccentric centre( $r_c/r_0$ ) and axial velocity gradient( $\Omega'_0$ ) at third bend inlet ( $\theta=0^\circ$ ), when three bends( $\theta_0=90^\circ$ ) are combined in a state of  $L_{m1}=L_{m2}=0$ .

$\psi^\circ$	45	90	135
$\alpha_0^\circ$	45	90	135
$\xi'_0$	0	0	0
$r_c/r_0$	0.04	0.04	0.04
$\Omega'_0$	0.3~0.6	0.3~0.6	0.3~0.6
R/d	3	1.5, 2, 3	3

Table 2 Direction of axial velocity gradient( $\alpha_0$ ), vorticity( $\xi'_0$ ), radial distance of eccentric centre( $r_c/r_0$ ) and axial velocity gradient( $\Omega'_0$ ) at second bend inlet ( $\theta=0^\circ$ ), when two bends( $\theta_0=90^\circ$ ) are combined in a state of  $L_{m1}=0$ .

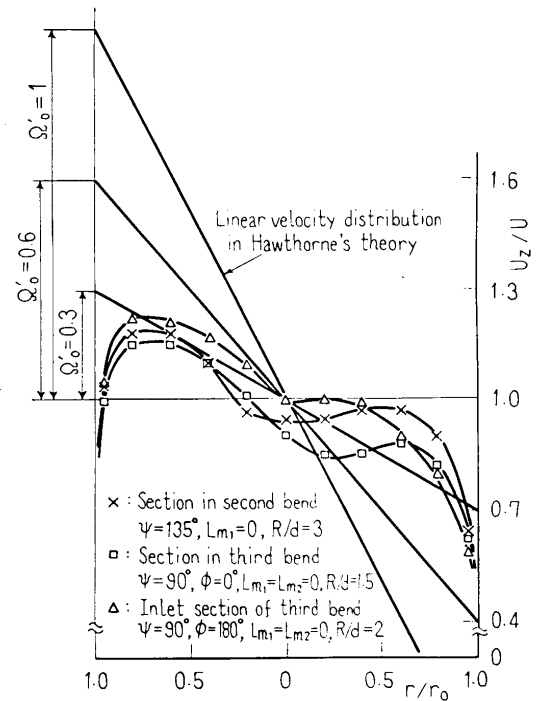


Fig.3 Measured axial velocity distributions

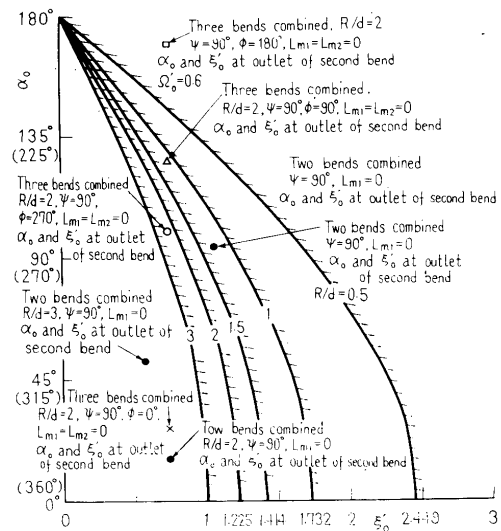


Fig.4 Relationship between vorticity  $\xi'_0$  and angle of eccentric centre  $\alpha_0$  at bend inlet, when  $4/KB=1$ . [Right hand side of these solid lines,  $4/KB < 1$ , corresponds to spiral swirling flow region. Left hand side,  $4/KB > 1$ , corresponds to oscillatory swirling flow region. • sign: values of  $\alpha_0$  and  $\xi'_0$  at outlet ( $L_d=0$ ) of second bend when two bends combined as  $\psi=90^\circ$ ,  $L_{m1}=0$ . x,  $\Delta$ ,  $\square$ ,  $\circ$  signs, respectively, show values of  $\alpha_0$  and  $\xi'_0$  at second bend outlet when three bends combined as  $\psi=90^\circ$ ,  $\phi=0^\circ$ ,  $90^\circ$ ,  $180^\circ$ ,  $270^\circ$ ,  $L_{m1}=L_{m2}=0$ ]

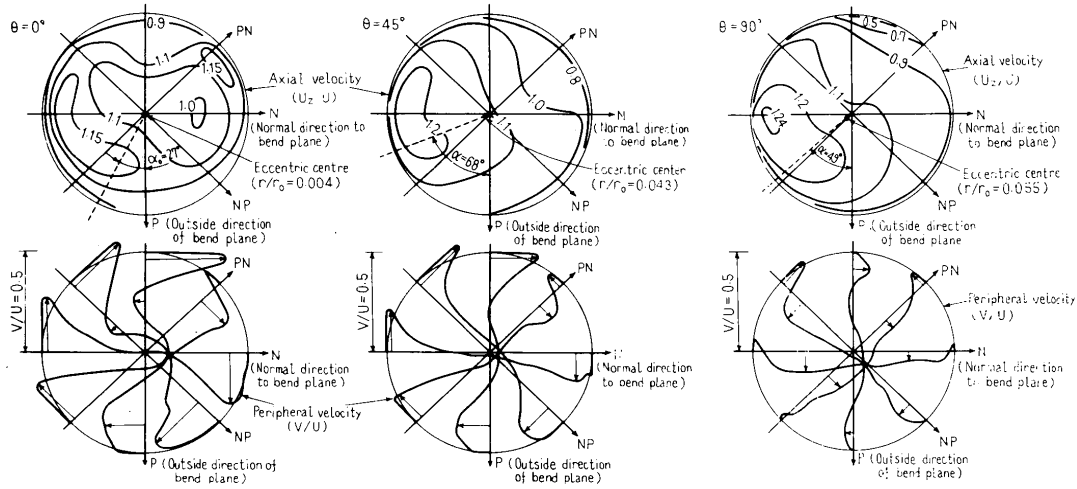


Fig.5 Velocity distributions in third bend, when three bends are combined in a state of  $\psi=90^\circ$ ,  $\phi=0^\circ$  and  $L_{m1}=L_{m2}=0$ . Deflection of bends  $\theta_0=90^\circ$ , bend radius  $R/d=2$ ,  $Re=10^5$

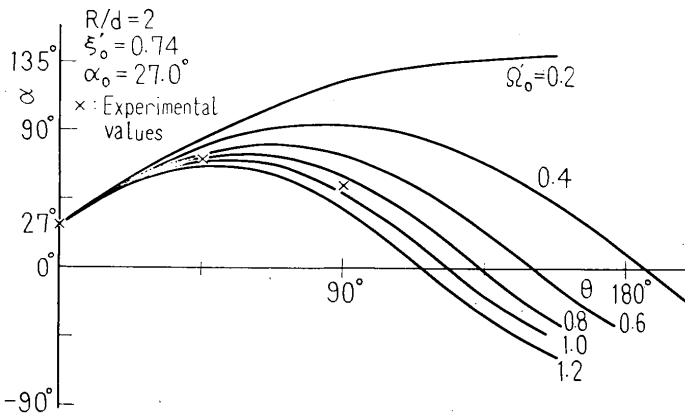


Fig.6 Variation of direction of axial velocity gradient  $\alpha$  along bend axis when  $4/KB > 1$  ( $R/d=2$ ,  $\theta_0=90^\circ$ ,  $\psi=90^\circ$ ,  $\phi=0^\circ$  and  $L_{m1}=L_{m2}=0$ ,  $Re=10^5$ )  
x : experimental values

## 6.2 Entry of non-uniform axial flow without swirling velocity component

As an example of this type flow, velocity distributions in the second bend are shown in Fig.9, when two bends are combined in a state of  $\psi=90^\circ$  and  $L_{m1}=0$ . The angular position of axial velocity centre  $\alpha$  moves on a sinuous path along the bend axis. The values of  $\alpha$  change from  $-90^\circ$  at the bend inlet  $\theta=0^\circ$  to  $-39^\circ$ ,  $61^\circ$ ,  $86^\circ$  and  $11^\circ$  successively through sections  $\theta=45^\circ$ ,  $90^\circ$ ,  $135^\circ$  and  $180^\circ$ . Thus, the plane of eccentric centre ( $\alpha$ ) changes in an oscillatory fashion in both sides of the bend plane  $\alpha=0^\circ$ , or P-axis. The relationship between  $\alpha$  and  $\theta$  in the second bend obtained by Eq.(30) is compared with experiments in Fig.10, where the theoretical results for different values of  $R/d$  are also plotted.

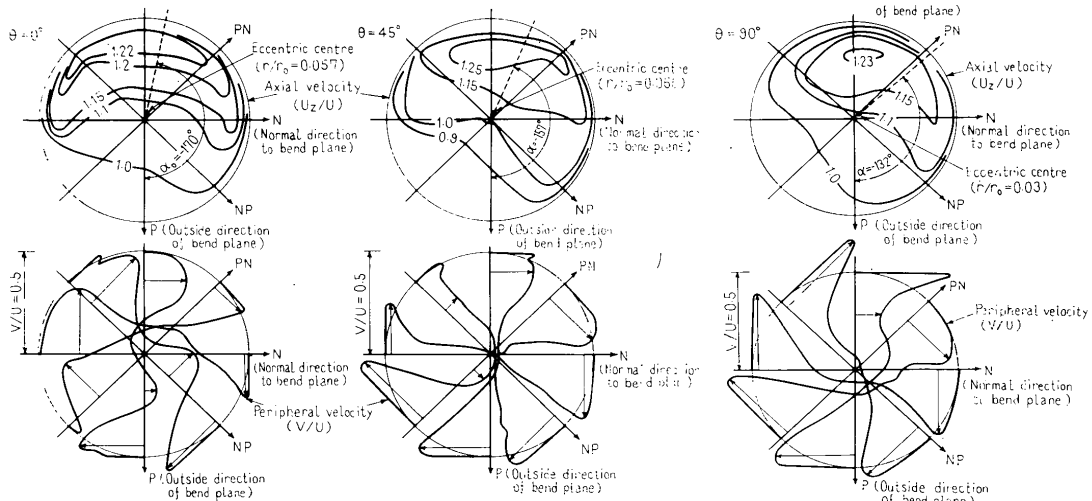


Fig.7 Velocity distributions in third bend, when three bends are combined in a state of  $\psi=90^\circ$ ,  $\phi=180^\circ$ ,  $L_{m1}=L_{m2}=0$ . Deflection of bends  $\theta_0=90^\circ$ , bend radius  $R/d=2$ ,  $Re=10^5$

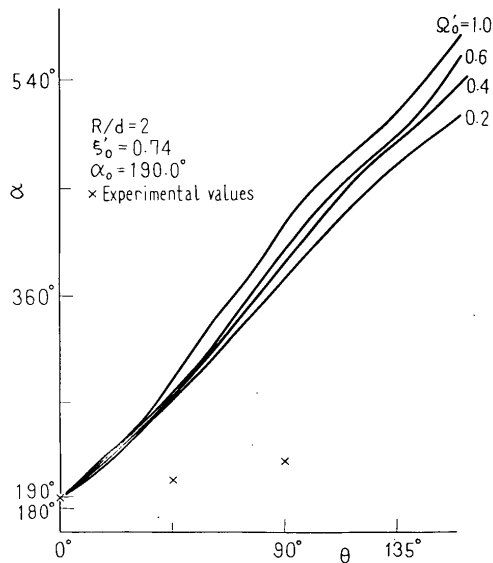


Fig.8 Variation of direction of axial velocity gradient  $\alpha$  along bend axis when  $4/KB < 1$  ( $R/d=2$ ,  $\theta_0=90^\circ$ ,  $Re=10^5$ ,  $\psi=90^\circ$ ,  $\phi=180^\circ$ ,  $L_{m1}=L_{m2}=0$ ) x: experimental values

The theoretical values by Eq.(30) with constants  $\alpha_0$ ,  $\xi_0$  and  $R/d$  together with  $\Omega_0=0.2\sim 1.2$  are shown by the full lines and the experimental values by the symbol x. When  $R/d=1.5$ , the theoretical values obtained with  $\Omega_0=0.6$  agree well with experimental ones over the whole range of  $\theta$ . When  $R/d=2$  or 3, however, the agreement is limited only to a small range and becomes poor within the range of  $\theta > 135^\circ$  ( $\Omega_0=0.6$ ). The discrepancy will be due to an increase of flow resistance, which is neglected in the theory, caused by an increased length of flow passage in large radius bends.

Hawthorne obtained the following expression for the flow in a bend, when an inviscid and incompressible shear flow with uniform pressure and an axial velocity varying in one direction only enters the bend

$$d\alpha/d\theta = [(2R/d) + \sin \alpha] \times [\ln\{1 + (d/2R) \sin \alpha\}]^{1/2} \quad (43)$$

where it is assumed that the maximum axial velocity is twice the mean velocity and the minimum velocity is zero for the inlet velocity distribution. This velocity distribution corresponds to that for  $\Omega_0=1$  in our theory, and this does not seem to be a proper assumption for the present flow as is seen in Fig.3.

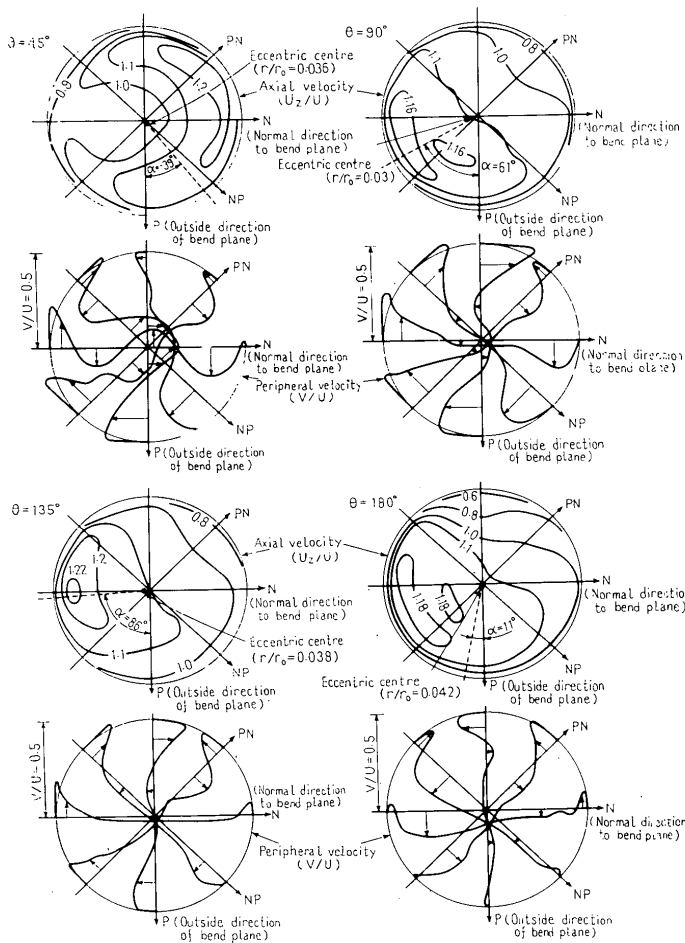


Fig.9 Velocity distributions in second bend, when two bends are combined in a state of  $\psi=90^\circ$ ,  $L_{m1}=0$ . Deflection of first bend  $\theta_0=90^\circ$ , deflection of second bend  $\theta_0=180^\circ$ , bend radius  $R/d=3$ ,  $Re=10^5$ .

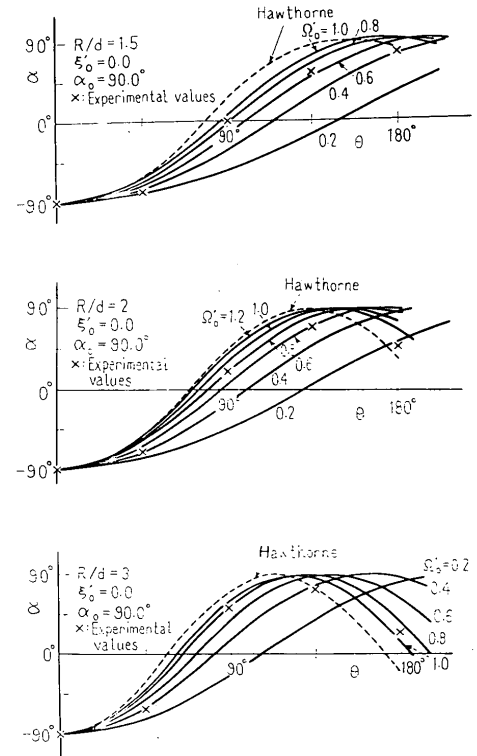


Fig.10 Variation of direction of axial velocity gradient  $\alpha$  along bend axis ( $4/KB > 1$ ). Experimental values correspond to those in second bend ( $\theta_0=180^\circ$ ) combined as  $\psi=90^\circ$ ,  $L_{m1}=0$  to first bend. Deflection of first bend  $\theta_0=90^\circ$ , deflection of second bend  $\theta_0=180^\circ$ ,  $Re=10^5$ . (a)  $R/d=1.5$ ,  $\xi_0=0$ ,  $\alpha_0=90^\circ$  (b)  $R/d=2$ ,  $\xi_0=0$ ,  $\alpha_0=90^\circ$  (c)  $R/d=3$ ,  $\xi_0=0$ ,  $\alpha_0=90^\circ$

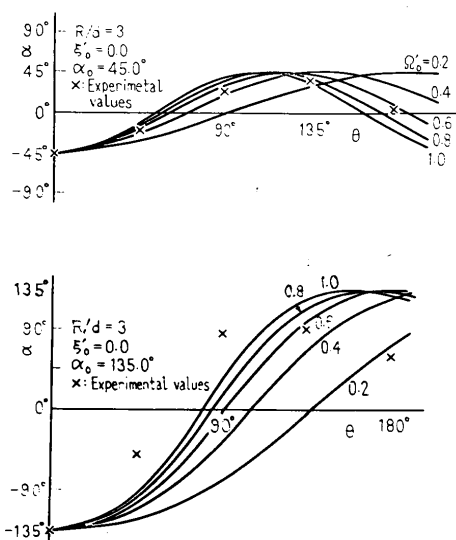


Fig.11 Variation of direction of axial velocity gradient  $\alpha$  along bend axis ( $4/KB > 1$ ). Deflection of first bend  $\theta_0 = 90^\circ$ , deflection of second bend  $\theta_0 = 180^\circ$ ,  $Re = 10^5$ . (a)  $R/d=3$ ,  $\xi_0=0$ ,  $\alpha_0=45^\circ$ , experimental values: in second bend combined as  $\psi=45^\circ$ ,  $L_{M1}=0$  to first bend. (b)  $R/d=3$ ,  $\xi_0=0$ ,  $\alpha_0=135^\circ$ , experimental values: in second bend combined as  $\psi=135^\circ$ ,  $L_{M1}=0$  to first bend.

It is clear in Fig.10 that Hawthorne's results agree well with the results for  $Q_0 = 1.0 \sim 1.2$  predicted by our theory. The effects of  $\alpha_0$  on the bend flow are also shown in Fig.10(c) and Fig.11. Agreement between the theory and experiments becomes better as the initial value  $\alpha_0$  decreases. This will be due to the same reason described in the end of Section 6.1.2.

## 7. Conclusions

- (1) The general behaviour of secondary flow in a bend was analyzed theoretically when a flow with non-uniform axial velocity together with a swirling component was introduced in the bend, and the following three types of flow were predicted to occur :
  - (1) oscillatory swirling flow
  - (2) spiral swirling flow
  - (3) suspended swirling flow

- (2) These results were confirmed by experiments and compared with results in the past investigations.

## References

- (1) Squire, H.B. and Winter, K.G., J. Aeron. Sci., 18. (1951-4), 271.
- (2) Hawthorne, W.R., Proc. Roy. Soc. Lond., Ser. A, 206-1086 (1951-5), 374.
- (3) Horlock, J.H., Proc. Roy. Soc. Lond., Ser. A, 234-1198 (1956-2), 335.